ORIGINAL RESEARCH

Pathological Comparison of Rat Pulmonary Models Induced by Silica Nanoparticles and Indium-Tin Oxide Nanoparticles

Yi Guan[1], Nan Liu[1], Yan Yu[1], Qiang Zhou[1,2], Meiyu Chang[1,2], Yongheng Wang[1], Sanqiao Yao[1,2]

[1]School of Public Health, North China University of Science and Technology, Tangshan, People's Republic of China; [2]School of Public Health, Xinxiang Medical University, Xinxiang, People's Republic of China

Correspondence: Sanqiao Yao, Email sanqiaoyao@xxmu.edu.cn

Purpose: The objective of this study was to evaluate and compare the histopathological implications of silica nanoparticles (Nano-SiO_2) and indium-tin oxide nanoparticles (Nano-ITO), in vivo.

Methods: Male Sprague-Dawley rats were exposed to Nano-SiO_2 (50 mg/kg) and Nano-ITO (6 mg/kg) by a single intratracheal instillation, respectively. Broncho-alveolar lavage fluid (BALF) and lung tissue were obtained at 7, 14, 28, and 56 days post exposure for analysis of BALF inflammatory factors, total protein, and for lung tissue pathology. Histopathological and ultrastructural change in lungs were investigated by hematoxylin and eosin, Masson's trichrome, sirius red staining, periodic acid Schiff stain, and transmission electron microscopy. The expression of SP-A, collagen type I and III in lung tissue was determined by immunohistochemistry and ELISA.

Results: The rats in both models exhibited obvious collagen fibrosis and the severity of the lung injury increased with time after exposure to respective dosage increased. Several parameters of pulmonary inflammation and fibrosis significantly increased in both groups, which was reflected by increased LDH activity, total proteins, TNF-α, and IL-6 levels in BALF, and confirmed by histopathological examination. The results also showed that the two models exhibited different features. Exposure to Nano-ITO caused persistent chronic lung inflammation, illustrated by the infiltration of a large amount of enlarged and foamy macrophages and neutrophils into the lung parenchyma. In Nano-SiO_2 exposed rat lung tissue, granulomatous inflammation was most prominent followed by progressive and massive fibrotic nodules. Compared with the Nano-SiO_2 rats, Nano-ITO exposed rats exhibited significantly severe pulmonary alveolar proteinosis (PAP) pathological changes, lower fibrosis, and higher levels of inflammatory biomarkers. However, Nano-SiO_2 exposed rats had greater fibrosis pathological changes and more severe granulomas than Nano-ITO exposed rats.

Conclusion: This study suggests that the Nano-SiO_2-induced model has greater value in research into granulomas and fibrosis, while the Nano-ITO-induced model has greater repeatability in area of PAP.

Keywords: silica nanoparticles, indium-tin oxide nanoparticles, silicosis, indium lung disease, pulmonary alveolar proteinosis

Introduction

Occupational exposure to contaminants is a substantial cause of respiratory disease globally. Occupational lung diseases are difficult to accurately enumerate, but are undoubtedly a sentinel health event that can strike an investigation into the cause and the implications for a population. Identification of a new occupational disease can take preventive intervention measures to further reduce the disease burden, and can also provide pathophysiological insights for known diseases.[1] Pneumoconiosis is still the best-known occupational chronic airway disease, and the risks arising from exposure to silica and asbestos are well known. However, with the emergence of innovative technologies, new threats are continually introduced into the workplace (such as indium compounds).[2–6] In 2017, Okamoto[7] first reported a case of pneumoconiosis in a dental technician related to indium exposure. Histological analysis of surgical lung biopsy specimens from this case showed peribronchiolar fibrosis with pigmented macrophages and cholesterol clefts. The histological findings of this

case are similar to those of indium lung disease. Some cases of indium lung disease might have been diagnosed as pneumoconiosis. Another example is the identification of a group of pulmonary fibrosis, emphysema, and pulmonary alveolar proteinosis (PAP) in indium-tin oxide (ITO) workers in the industry of flat-panel display manufacture (eg liquid-crystal or plasma screens for televisions).[8] It is worth noting that the International Agency for Research on Cancer (IARC) of the World Health Organization recently classified ITO as a possible carcinogen (Group 2B) based on sufficient evidence from animal experiments to warrant tighter exposure control measures in workplaces.[9]

Silica, an abundant occupational hazard which has been studied for more than 100 years, still gives rise to new cases of silicosis despite regulations and strategies for controlled exposure, partly because of non-conventional sources of exposure. Silica is the main cause of occupational respiratory diseases all over the world. At present, it is recognized as a lung carcinogen. ITO has become a new occupational hazard, which can induce indium lung disease. As early as one year after first exposure, indium lung disease can occur without a clear work-related cause and is marked by cough, dyspnea, and abnormalities evident from pulmonary function tests and chest CT.[10] Available evidence shows that indium lung disease begins with PAP, progresses to fibrosis and emphysema, and is followed by high rate of morbidity and mortality. Although intensive efforts have been made, there are still no effective therapies. One of the most important reasons is that models are not perfect, and they can have difficulty imitating pathologic changes. Additionally, the majority of researchers focused on the effects on animals at a single time point, whereas indium lung disease may have unique physiological effects at different phases of the diseases. The purpose of this study is to compare and analyze the causal relationship of the major lung diseases caused by silica (classic forms of hazardous exposure: silicosis) and ITO (newly identified exposure sources: indium lung), and to discuss possible avenues for their identification and prevention.

Here, we investigated, at different times after exposure, pulmonary toxicity of silica nanoparticles (Nano-SiO$_2$) and ITO nanoparticles (Nano-ITO). Nano-SiO$_2$ is already widely used in manufacturing processes and electronic products. In recent years, Nano-ITO has also attracted attention in biomedical applications, yet its toxicity has not been fully understood. The applications of nanomaterials in various fiels like superhydrophobic surfaces, inorganic electronics, organic electronics, batteries, etc, are inevitable and have become part of our day to day life.[11,12] The aim of the novel research presented in this study is to expand upon previous research results by evaluating histopathological implications of the two rat models, using samples taken from multiple areas of the lung at several time-points after intratracheal instillation with Nano-SiO$_2$ and Nano-ITO. We hope to draw a clearer picture of their characteristics and have a better understanding of the disease mechanism.

Materials and Methods
Experimental Animals
One hundred and twenty-eight male specific-pathogen-free (SPF) Sprague-Dawley rats, weighing 160–190 g, were purchased from the Medical Laboratory Animal Center of North China University of Science and Technology. Rats were maintained in standard housing conditions (temperature: 25±1°C, relative humidity: 50±5%; light and dark cycle: 12h:12h) and had free access to standard rat chow and water. Food (sterile feed) and water (through automatic watering system) were provided ad libitum. Before the experiment, the rats were adapted to the animal facility for 1–2 weeks, and their overall health status was monitored daily. All procedures used in this study were conducted in accordance with the Guide for the Care and Use of Laboratory Animals Center of North China University of Science and Technology and approved by the Experimental Animal Ethics Committee of North China University of Science and Technology (Permit No. 2017011).

Reagent Preparation
Nano-SiO$_2$ and Nano-ITO were purchased from Sigma and Aladdin. Before intratracheal instillation, both were suspended in sterile physiological saline respectively. The microstructure, surface morphology and relative size of Nano-SiO$_2$ and Nano-ITO were measured by transmission electron microscopy (TEM). The dispersion of Nano-SiO$_2$ and Nano-ITO were measured by granulometer (Malvern Mastersizer2000, Britain).

Intratracheal Instillation Experiments

The Nano-SiO$_2$ sample (50 mg/kg) and Nano-ITO sample (6 mg/kg) were suspended in saline sterilized by autoclave, and then penicillin was added to a final concentration of 8000 U/mL. The suspension was dispersed by vortex shaker before administration in rats.

The rats were instilled intratracheally following previously described procedures.[13] Briefly, rats were deeply anesthetized with isoflurane until fully relaxed. A plastic syringe was intubated into the trachea and a suspension of Nano-SiO$_2$ or Nano-ITO was instilled at a volume of 1 mL.

Rats were randomly divided into the following two experimental groups: (1) Nano-SiO$_2$ group (n=64); (2) Nano-ITO group (n=64). The control group of rats received 1 mL of 0.9% saline by intratracheal administration (added with penicillin to a final concentration of 8000 U/mL); rats in the Nano-SiO$_2$ group were administered a single intratracheal instillation of Nano-SiO$_2$ suspension (1 mL, 50 mg/kg); for the rats in the Nano-ITO group, a one-time dose of 6 mg/kg ITO was intratracheally instilled. After the procedure, each rat was weighed and transferred to the animal facility. Animals were sacrificed on day 7, 14, 28 and 56 after intratracheal instillation. The blood samples collected from ventral aorta were centrifuged at 3000 × g for 10 min at 4 °C. Serum was separated, placed in a centrifuge tube, and stored at −80°C. The bronchoalveolar lavage fluid (BALF) was collected by lavaged three times with 5 mL sterile saline and centrifuged at 1000 × g for 10 min at 4 °C, and the supernatant was stored at −80 °C. Lungs were then removed and rinsed three times with normal saline for complete blood removal. The right lungs were dissected and used for histopathological staining and immunohistochemistry. The left lungs were frozen and stored at −80 °C for biochemical analysis. Each experimental group included eight animals.

Histopathological and Immunohistochemistry Analysis

Four rats from each control and model group were used for lung histopathological assessment. The selected lung tissue sections were put into embedding cassettes and soaked in 10% neutral-buffered formalin for fixation. The fixed tissues were routinely treated and embedded in paraffin for histopathological examination. Tissue sections (5 μm thick) were cut and stained with hematoxylin and eosin (H&E) to visualize pulmonary inflammatory infiltration. In addition, the embedded lung tissues were cut into 3 μm thick sections and stained with Masson's trichrome to indicate lung fibrosis, sirius red staining for the location of collagen deposition in the lung, which was stained in red, and periodic acid Schiff (PAS) stain to show alveolar protein deposition. Tissue sections were evaluated using light microscopy.

SP-A and collagen I were assessed by immunohistochemistry. Briefly, lung tissue sections were stained using the immunohistochemical envision two step method. Fresh lung tissue was dissected with paraformaldehyde, fixed at 4°C, paraffin embedded, serially sectioned, and dewaxed. A 3% hydrogen peroxide solution was used to remove endogenous peroxidase, followed by washing three times with PBS. The antigens were retrieved by heating the tissue sections in citrate buffer in microwave. Then they were immunostained with avidin biotinylation enzyme complex antibodies. Polyclonal rabbit anti-SP-A (Affinity, 1:150) and anti-collagen type I (Affinity, 1:100) were used as primary antibodies. The lung tissues were incubated with those primary antibodies overnight at 4 °C, and then with horseradish peroxidase polymer secondary antibodies at room temperature for 1 h. The slices were washed three times with PBS. DAB is used as developer for color development. Positive cells were stained brown by DAB in the cell nucleus and cytoplasm. Image-Pro Plus 6.0 software was used for quantitative analysis of immunohistochemical staining. Three slices of each animal were evaluated to obtain a mean value. After segmentation, the mean intensity of the positive cell regions was measured blindly.

Transmission Electron Microscopy (TEM)

The right lungs from two rats per group from each sample time point were taken for ultrastructure analysis by TEM (JEM-100CX, Japan). The lung tissues were fixed using glutaraldehyde and osmium tetroxide solution, dehydrated in ethanol, and embedded in epoxy resin. At room temperature, ultrathin sections of lung tissue were stained with 2% uranyl acetate solution and 0.5% lead citrate solution and examined for particle deposition and PAP, and its relation to alveolar macrophages (AM).

Analysis of Pulmonary Injury and Inflammatory Cytokines in BALF

In order to evaluate cytotoxicity as a measure of lung damage, lactate dehydrogenase (LDH) activity and total protein (TP) levels in the BALF of all exposed groups were measured at each time point after exposure. LDH activity in the BALF was measured by LDH cytotoxicity test kit. The TP concentration in the BALF was determined by the Bradford method and Bio-Rad Protein Assay. The levels of pro-inflammatory and anti-inflammatory cytokines in BALF, including tumor necrosis factor (TNF)-α and interleukin (IL)-6, were measured using enzyme-linked immunosorbent assay (ELISA) kits (Nanjing Jiancheng Bioengineering Institute, Nanjing, China), according to the instructions provided.

Analysis of Enzyme-Linked Immunosorbent Assay (ELISA)

Lung tissues were homogenized in buffer and centrifuged (at $3000 \times g$ for 10 min) to obtain liquid supernatants. According to the manufacturer's instructions (Shanghai, China), the levels of SP-A, collagen type I and collagen type III in the supernatants were evaluated by ELISA. Optical density at 450 nm was measured with a microplate reader (Thermo, USA) and the antigen level (in ng/L) was calculated. The protein concentration (in mg/mL) of the corresponding supernatant were determined with BCA Kit (Nanjing Jiancheng Bioengineering Institute, Nanjing, China), and normalized the relative content (in ng/g) of SP-A, collagen type I and collagen type III in each sample.

Statistical Analysis

Data were expressed as mean ± SD. The results of the Nano-SiO$_2$ and Nano-ITO groups were compared to those of the corresponding negative control group. One-way analysis of variance (ANOVA) was used for statistical comparison, followed by Bonferroni t-test or Dunnett's t-test. The statistical significance level was assigned at a probability value of $P < 0.05$. Statistical analyses were conducted by using SPSS 21.0 software.

Results

Characterization of Nanoparticles

The size and morphological characteristics of Nano-SiO$_2$ was examined using a high-resolution TEM, and images exhibited a relatively regular morphology and mild aggregation phenomena (Figure 1A). We also assessed the hydrodynamic diameters of Nano-SiO$_2$ and found that the peaks of the silica nanoparticle size were distributed at 763.2 nm, and the average particle size is 49.62 ± 2.49 nm. Meanwhile, TEM revealed Nano-SiO$_2$ aggregates, black dots, in the lungs of rats exposed to Nano-SiO$_2$ for 56 days (Figure 1B). The Nano-ITO used in this study were characterized as previously described.[13] The TEM images are presented in Figure 1C and show that the Nano-ITO was nearly spherical or ellipsoidal in shape. The average size of the Nano-ITO was 55.3±1.1 nm, while the peaks of the Nano-ITO particle size was distributed at 785.12 nm, which indicated that the nanoparticles were agglomerated, but it can be easily dispersed by simple sonication. Figure 1D shows a TEM image of the presence of dispersed Nano-ITO in the alveolar space and alveoli.

Body Weight

No rats died during the intratracheal instillation period. No systemic signs such as respiratory distress, or behavioral disorder were apparent during the experimental period in both groups. Following intrathecal instillation of Nano-SiO$_2$ or Nano-ITO, the mental status, fur, behavior, food intake, urine, and feces of rats were observed weekly. No unusual changes were detected. The body weight of Nano-SiO$_2$-exposed groups and the control group showed similar increasing trends throughout the experimental period, but significant decreasing in the 56 day Nano-SiO$_2$ group (Figure 2). No statistically significant differences in body weight were observed between Nano-ITO groups and controls at four time points. These results indicated that Nano-SiO$_2$ interfered with the growth of rats, but Nano-ITO did not.

Macroscopic and Microscopic Observation of the Lungs

The results showed a significantly different histopathological change was observed between the Nano-SiO$_2$ and Nano-ITO group when compared with the control group at each sample time point.
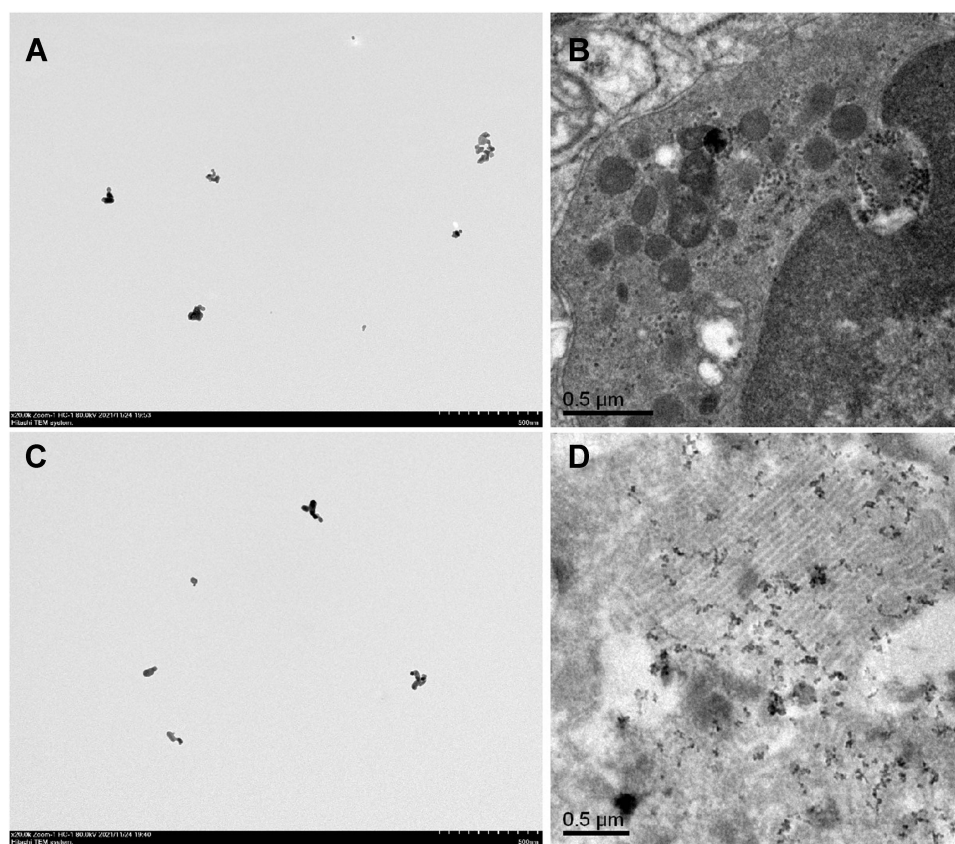
Figure 1 The characterization of Nano-SiO$_2$ and Nano-ITO. (**A**) The TEM images of the Nano-SiO$_2$, with scale bars of 500 nm. (**B**) Nano-SiO$_2$ bioaccumulate in lung tissues by TEM analysis. Scale bar = 0.5 μm. (**C**) TEM images of the Nano-ITO, with scale bars of 500 nm. (**D**) Nano-ITO bioaccumulate in lung tissues by TEM analysis. Scale bar = 0.5 μm.
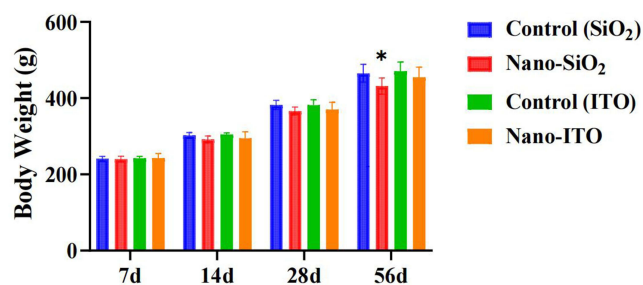
Figure 2 Body weight of rats exposed to Nano-SiO$_2$ and Nano-ITO. Results are expressed as mean ± SD and analyzed using One Way ANOVA followed by Bonferroni's post-hoc test at $P < 0.05$ (n = 8). *Indicates significant differences from control rats.

In regard to macroscopic findings, the lungs in the control group were soft and elastic, and the surfaces were lustrous; in the Nano-SiO$_2$ groups, the surfaces of the lungs had white spots and pulmonary hemorrhage. In Nano-SiO$_2$ groups at day seven and day 14, the lungs were congested, swollen, and slightly enlarged. In the 28-day Nano-SiO$_2$ group, obvious pulmonary edema was observed, accompanied by a small amount of dark red hemorrhagic areas, and scattered tip and millet gray white spots on the lung surface. In the 56-day Nano-SiO$_2$ group, the elasticity of the lungs was significantly worse, the color of their surfaces was gray-white and obvious scattered protrusions, they were hard to the touch and felt gravelly when cut. In the control group, the pathologic images of lung tissue stained with H&E showed that the lung tissue was normal, alveolar wall was thin, and the alveolar structure was clear and intact. After seven days, there was a large amount of infiltration of inflammatory cells (neutrophils and macrophages) in alveolar spaces. The alveolar wall began to thicken. In the lung tissue of the 14-day Nano-SiO$_2$ group, the epithelioid cells and macrophages

of the tubercle accumulated to form nodules, surrounded by leukocyte infiltration, the rupture of the pulmonary septal and severe congestion of capillaries and arterioles were visible. After 28 days, the lung tissue was severely damaged, the structure of the lungs was disordered, and the lung tissue was filled with concentric tubercles. And in those of the 56-day Nano-SiO$_2$ group, macrophages in the damaged lung tissue formed cell nodules, caseous necrosis increased, and collagen fibers proliferated. The walls of small vascular in the middle of the giant fibrous nodules are thickened, and the proliferated endothelial cells were arranged in concentric circles. Furthermore, there were destruction of alveolar structures, form of spindle fibroblasts and thickening of the interstitial lung. The changes were more significant as time after exposure to Nano-SiO$_2$ increased (Figure 3A).

Compared with the control group, the lungs of rats instilled with Nano-ITO in the intratracheal showed extensive dark red hemorrhages, indicating that the lungs had severe inflammatory lesions (Figure 3B). After seven days, the color of both lungs in the Nano-ITO exposure group deepened; after 14 days, the volume of both lungs in the Nano-ITO exposure group was slightly larger than that in the control group, with diffuse bleeding, deepened color and tight pulmonary capsule; after 28 days, in the Nano-ITO exposure group, both lungs were significantly swollen and the volume increased, large irregular white plaques could be seen on the surface of the lungs, and a small number of bleeding spots appeared on both lungs; on the 56th day, in the Nano-ITO exposure group, the color of both lungs was dark red, and the lung capsule was tight. Spongy changes, flake bleeding and punctate white spots appeared. Diffuse punctate hemorrhage, focal hemorrhage and diffuse grayish white nodules are distributed on the edges of lungs. By contrast, lung histopathology of the Nano-ITO group was characterized by the presence of aggregated Nano-ITO around the alveolar duct and adjacent alveoli, and by induction of inflammation, small granulomas, destruction of AMs, and PAP. The acute inflammation was high at day seven. The granuloma persisted throughout the observation period and lasted until day 56. After 14 days of exposure to Nano-ITO, the incidence of inflammatory cell infiltration into the alveolar cavity and interstitial fibrosis was significantly increased, and there was diffuse alveolar injury characterized by type II pulmonary cell abscission and red blood cell extravasation. Furthermore, there were pulmonary abscesses with neutrophils, apoptotic debris and central necrosis, as well as peripheral bronchopneumonia and fibrosis in the 28 day Nano-ITO group. Notably, PAP occurred on day 28, and its severity gradually increased with time after instillation. Fibroblastic foci and honeycomb cysts were more frequently seen in the 56 day Nano-ITO group, with proteinous exudate inside multiple alveoli. Under the microscope, it was observed that there were eosinophilic particles in the honeycomb cysts.

Fibrosis, Collagen Deposition and Alveolar Protein Observation of the Lungs

Time dependent fibrosis was observed in the lungs of the rats exposed to Nano-SiO$_2$, which was characterized by the formation of nodules composed of granulomas, adjacent type II epithelial cell proliferation, fibroblast proliferation, and bundles of interlacing collagen fibers, as well as progressive massive fibrosis (Figure 4A). In the images of Masson's trichrome staining, the alveolar structure of the lung tissue in the control rats was clear, and there were a small amount of collagen fibers around the bronchus and blood vessels. Compared with the control group, the level of collagen deposition in the Nano-SiO$_2$ groups increased significantly at each time group. After 14 days exposure to Nano-SiO$_2$, there was a large number of infiltrating cells in the lungs of rats, the alveolar wall began to thicken, and collagen fibers increased. The results observed after 28 days were consistent with those in the 14 day groups. The number of inflammatory cells increased, collagen fibers increased, and alveolar walls thickened. After 56 days, collagen fibers fused into clusters, the alveolar wall became significantly thicker, and there were collagenous nodules with pigment-laden macrophages. The lung sections stained with sirius red to tint the collagen red, showed large red regions in the lungs at day 56 after Nano-SiO$_2$ exposure, suggesting deposition of collagen (Figure 4A). One of the most characteristic lesions demonstrated in the Nano-SiO$_2$ group was the presence of multiple non-caseating granuloma embedded in the pulmonary parenchyma. However, no PAS staining positive substance was found in the lung tissue of the Nano-SiO$_2$ exposure groups, indicating that there was no alveolar proteinosis in Nano-SiO$_2$ experimental rats.

The increase of collagen fiber was slightly obvious with the extension of time after exposure to the Nano-ITO increased, confirmed by Masson's trichrome and sirius red staining. The alveolar wall became widened, neutrophils infiltrated the lung tissue and inflammatory cells were exuded after day seven from exposure to Nano-ITO. Macrophages cellular nodules and collagen deposition appeared in the lung tissue of rats after day 14 from exposure to Nano-ITO.
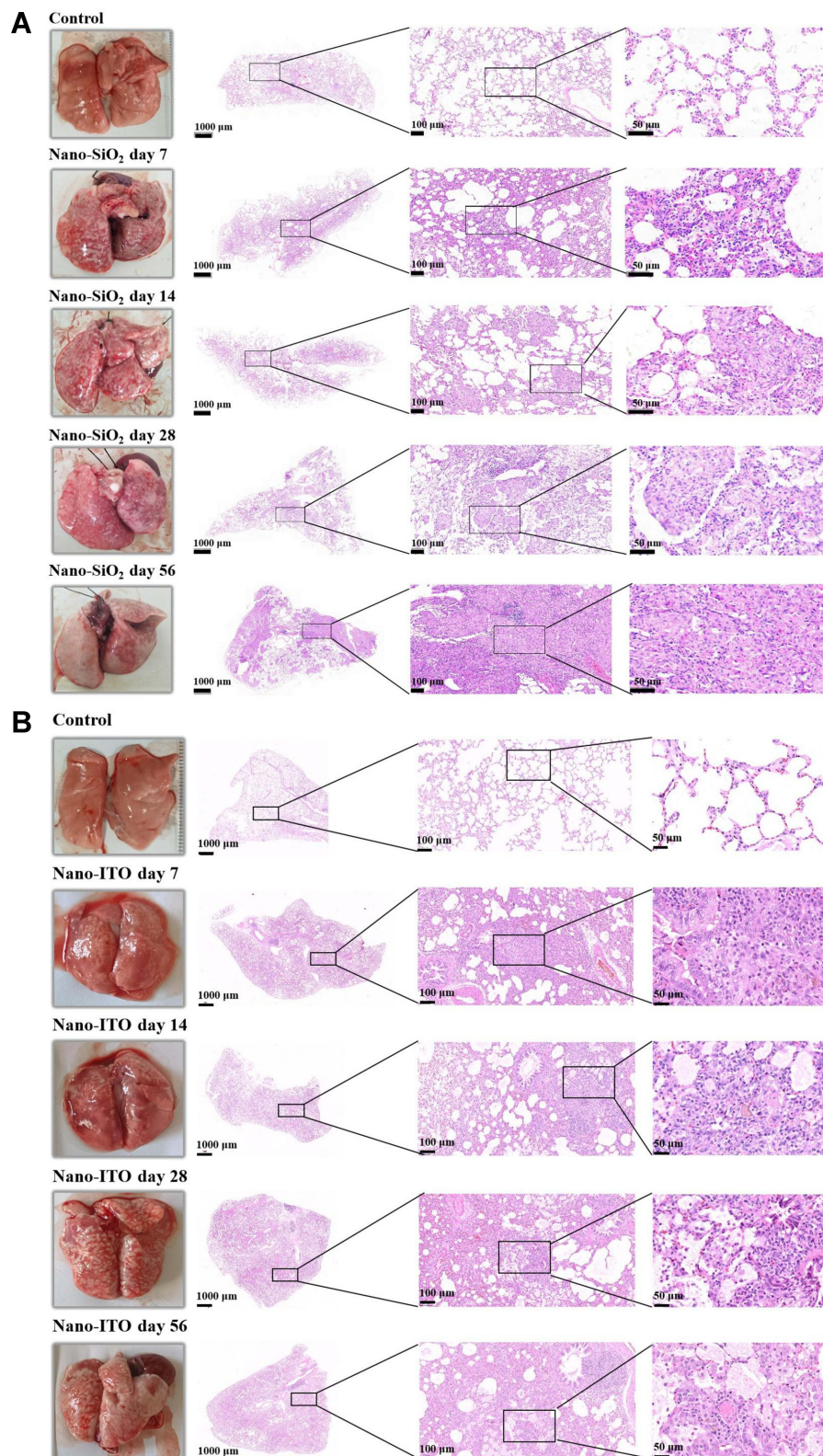
Figure 3 Comparison of gross appearance and pathological morphology changes in lungs of rats exposed to Nano-SiO$_2$ and Nano-ITO. (**A**) Nano-SiO$_2$ group: H&E staining indicated that inflammatory reaction appeared at day seven, isolated nodules were visible in lung tissue at day 14 and multiple cellular nodules formed at day 28; the multiple nodules were fused and huge fibrous nodules with diffuse interstitial fibrosis were observed at day 56 in the rats. (**B**) Nano-ITO group: The inflammation persisted throughout the whole observation period from the day seven to 56; PAP occurred on day 28, consisting of alveolar spaces filled with eosinophilic proteinaceous material and intraluminal aggregation of foamy macrophages.
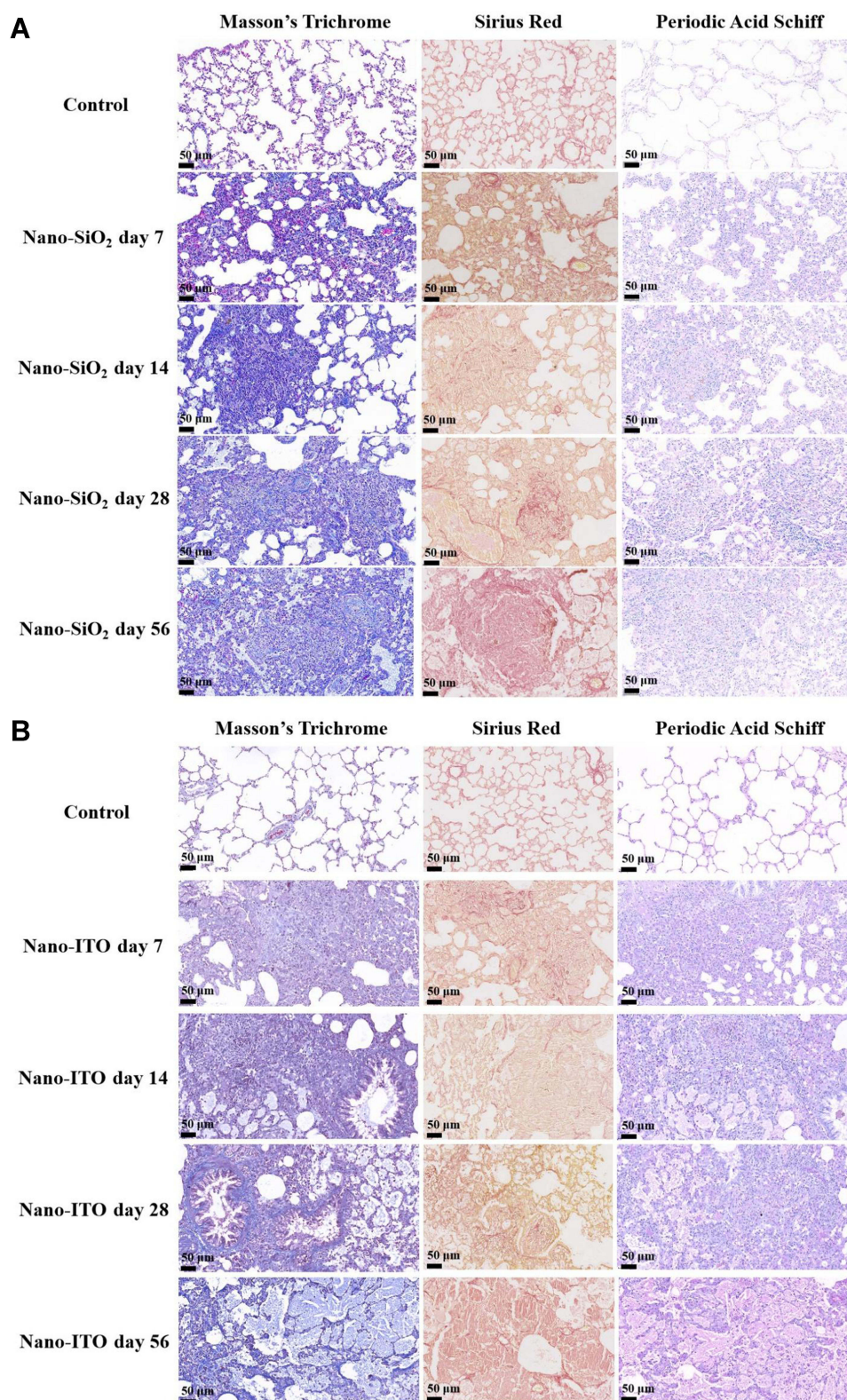
Figure 4 Comparison of pathologic images of fibrosis and alveolar protein of lung tissues stained with Masson's trichrome, sirius red, periodic acid Schiff. (**A**) Nano-SiO$_2$ group: Dense collagenous nodule with inner Nano-SiO$_2$-laden macrophages; the area of collagen stained in red significantly increased on day 56. (**B**) Nano-ITO group: After 28 days, proteinous exudate inside multiple alveoli and occasional foamy macrophages. Dense eosinophilic amorphous body, cholesterol clefts, and foamy macrophages inside the proteinous exudate frequently seen in the 56-day Nano-ITO group.

Multifocal proteinosis was demonstrated adjacent to the severely remodeled lung area at 28 days in the Nano-ITO group (Figure 4B). In the 56 day Nano-ITO group, alveolar macrophage migration, alveolar wall fibrosis, type II epithelial cell proliferation/hypertrophy, perivascular inflammation and collagen deposition were more significant. PAS staining showed that neutrophilic inflammation was observed on day seven and deteriorated to day 14, and severe PAP was observed on days 28 and 56. The 7-day Nano-ITO group were associated with collection of neutrophils. PAS staining in the lung specimens at day 14 showed accumulations of intra-alveolar lightly eosinophilic finely granular materials. In addition to this, a protein substance was observed in the alveolar spaces of Nano-ITO-exposed rats at day 28 post-exposure which always existed and was at higher levels at day 56 post-exposure. At the same time, the frequent foamy macrophages and cholesterol clefts as well as occasional dense eosinophilic amorphous bodies was also observed in the 56-day Nano-ITO group.

Observation by Transmission Electron Microscopy

The ultrastructural changes of lung tissue in each group were the same as the intuitionistic indicators of histomorphological changes. The TEM showed that the structure of lung tissue in the control group was clear, the alveolar type I cells were elongated, the alveolar type II cells were oval, and there were a large number of nuclei and villi on the cell membrane (Figure 5A). Compared with the control group, there was a significant inflammatory reaction in the 7-day Nano-SiO$_2$ exposure group for macrophages and infiltrating cells, and slight fibrosis was found. After 14 days, it was observed that the nuclei of alveolar type II cells was large, there were a few lamellar bodies in the cells, and the villi on the membrane fell down and fell off; there was a small amount of fibrosis around alveolar type II cells; there were many exfoliated cells around the lung stroma, and the inflammatory reaction was serious. In the 28-day group, the alveolar type II cells with a large nucleus and fuzzy nuclear membrane could be observed. There was obvious fibrous hyperplasia in the left and lower parts of alveolar type II cells, which contained a large number of osmiophilic lamellae dissociated in the alveolar cavity. There were exfoliated cells around the lung stroma, and inflammation was reduced compared with that in the 14-day group. In the 56-day group, the field of view was full of fused hyperplastic fibers. At the lower left of the section, the remaining alveolar type II cells, which were partially fibrotic, were observed. Mild hyperplastic type II alveolar epithelial cells contained large amounts of osmiophilic lamellar bodies. The macrophages increased and phagocytized osmiophilic lamellar bodies and Nano-SiO$_2$, which contained vesicles, lamellar bodies, collagen fibers
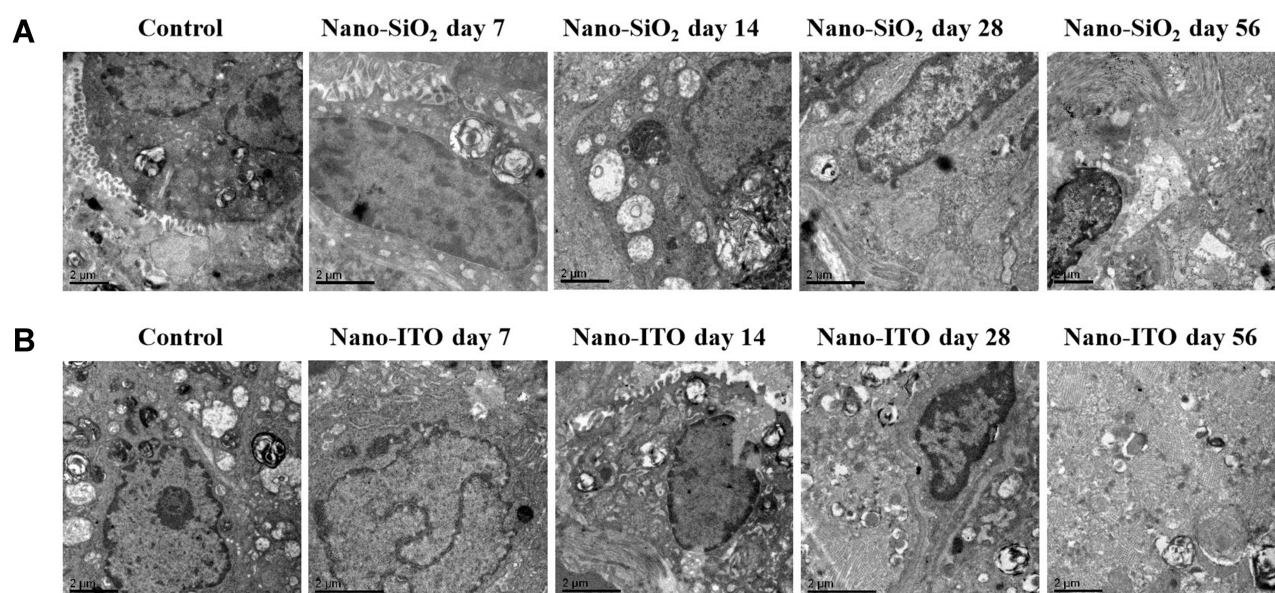
Figure 5 TEM images of lung tissues in rats with Nano-SiO$_2$ and Nano-ITO (bar =2 μm). (**A**) The fibrotic lesions in the Nano-SiO$_2$ group demonstrated elongated cells with lamellar bodies (characteristics of alveolar type II epithelial cells) and abundant rough endoplasmic reticulum and mitochondria (characteristics of fibroblasts). (**B**) TEM performed on lung tissues of Nano-ITO group showed the characteristic myelin-like whorled membranous structures which represent surfactant.

and elastic fibers. Some researchers have pointed out that hyperplastic alveolar type II cells were the initial events, and hypertrophic AMs was the key link to the development of pulmonary fibrosis in experimental silicosis.[14]

In comparison, TEM examination of the lungs from the Nano-ITO revealed that the protein deposition together with the Nano-ITO were gathered in the alveolar cavity. A significant inflammatory reaction was observed in the 7-day group for macrophages and infiltrating cells, and the blurred nuclear membrane; there was obvious fibrous hyperplasia, lodging and falling off of villi on the membrane at 14 days. Compared with the 14 day group, the fibrosis of lung tissue in the 28-day group was reduced, and the inflammation was further aggravated, with fine fibrillar component and amorphous dense substances. On the 56th day, TEM images of the lungs in the Nano-ITO group revealed that there were large-size, degenerative AMs that were phagocytosing the Nano-ITO particles, cellular debris, and protein substances. These materials were identified as the pulmonary surfactant, because of its crystalline or concentric layered structures, multi-layer, lattice-shaped and myelin-like structure (Figure 5B). Proteinaceous material found in the pulmonary alveoli of the Nano-ITO group were also confirmed by PAS staining.

Pulmonary Inflammation Responses

We measured the concentration of LDH released into BALF at seven, 14, 28, and 56 days post-exposure as a biomarker for lung cell injury. Assessment of the BAFL from Nano-SiO$_2$ and Nano-ITO exposure showed that Nano-SiO$_2$ increased the LDH release in a time-dependent manner (Figure 6A). Nano-SiO$_2$ appeared to be more cytotoxic. Because the Nano-SiO$_2$ was higher for LDH, this would indicate that the cell membrane integrity was more sensitive to Nano-SiO$_2$ exposure than to Nano-ITO exposure. As shown in Figure 6B, TP concentration in the BALF increased significantly at all time points after the instillation between the Nano-SiO$_2$ and the control. However, Nano-ITO induced more TP production than Nano-SiO$_2$ at all time points, indicating that Nano-ITO exposure caused more significant lung edema than Nano-SiO$_2$ exposure, which was consistent with PAS staining response.

Perturbation of cytokines excreted into BALF reflect inflammatory response of the lung to Nano-SiO$_2$ and Nano-ITO. Concentrations of IL-6 and TNF-α in BALF were then detected and compared at four time-points. ELISA results showed that the concentration of IL-6 and TNF-α in BALF were slightly significantly higher in rats challenged with Nano-SiO$_2$ and Nano-ITO compared with the control ($P<0.05$; Figure 6C and D). H&E staining results of lung tissue exposed to
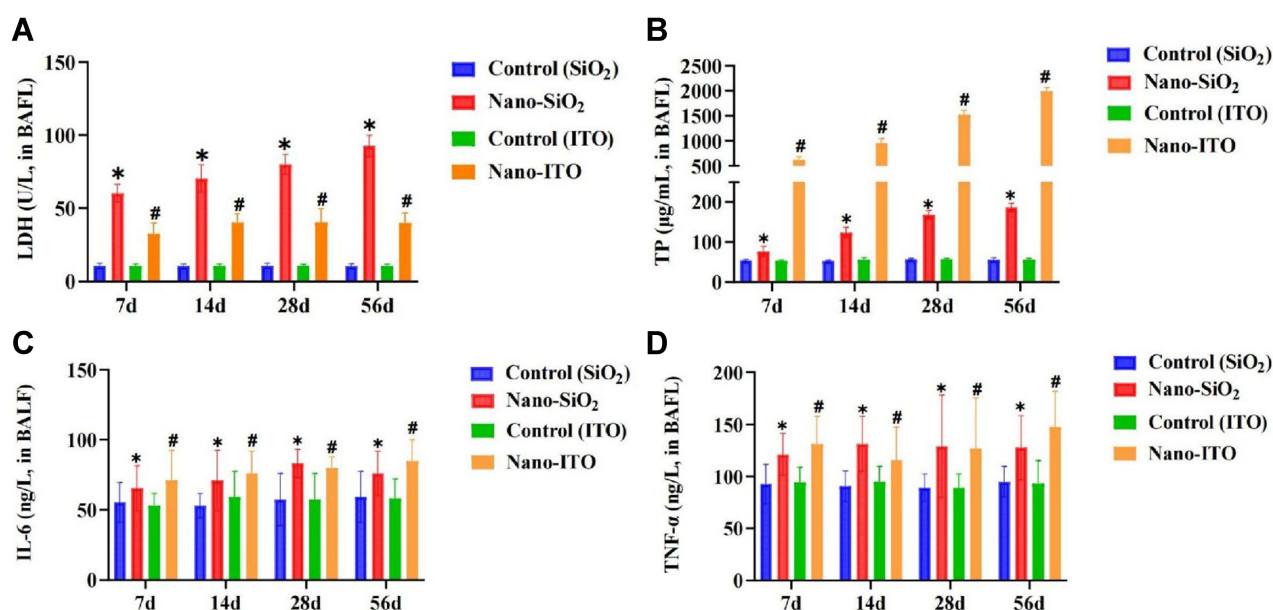

Figure 6 Markers for pulmonary injury (LDH and TP) and inflammation (IL-6 and TNF-α) in BALF. (**A**) LDH activity in the BALF. (**B**) TP concentration in the BALF. (**C**) IL-6 level in the BALF. (**D**) TNF-α level in the BALF. *$P < 0.05$, Nano-SiO$_2$ vs control, #$P < 0.05$, Nano-ITO vs control.

Nano-SiO$_2$ and Nano-ITO revealed that lung inflammation was induced in a time-dependent manner, which further verified the above findings that inflammation began at day seven (Figure 6).

Effects of Pulmonary Surfactant Protein

We hypothesized that Nano-SiO$_2$ or Nano-ITO may damage epithelial cells in rat lungs. To test this hypothesis, we performed immunohistochemistry using SP-A, a marker that reflects the epithelium of lung tissue in rats administered with Nano-SiO$_2$ or Nano-ITO. SP-A expression in normal lung tissue was high, which was observed in alveolar type II cells and some macrophages as brownish yellow granules. Figure 7 shows SP-A localization in the rat lung. As expected, there were a large number of SP-A positive cells on the alveolar wall surface of the control groups (Figure 7A). SP-A expression in Nano-SiO$_2$-treated rat lung at seven and 14 days was not significantly different compared with the control group. In contrast, SP-A positive cells in Nano-SiO$_2$ 28- and 56-day groups decreased significantly ($P <0.01$), while SP-A positive cells in the Nano-ITO groups were more, which revealed that Nano-ITO within alveolar spaces were strongly positive for SP-A; type II lung cells surrounding PAP-like changes were also positive for SP-A (Figure 7B). These results were supported by ELISA analysis (Figure 7C), which revealed decreased levels of the epithelial cell marker (SP-A) in Nano-SiO$_2$ 28- and 56-day groups. Conversely, Nano-ITO groups exhibited distinctly increased levels of SP-A. PAS staining showed that there were eosinophilic fine particles in the accumulated substances of the Nano-ITO group. Lung tissue SP-A immunohistochemistry was significantly positive in the Nano-ITO group but not in the Nano-SiO$_2$ group. In sharp contrast, serum SP-A levels distinctly increased only in the Nano-SiO$_2$ group, although interestingly, they were significantly decreasing in the Nano-ITO group (Figure 7D). These findings suggested that SP-A, in Nano-ITO-exposed rats, was mainly present in the lung tissue, whereas it was in the serum of Nano-SiO$_2$-exposed rats. This finding was fascinating, which may be due to the circulation of SP-A in the bloodstream. The present findings suggested that lung tissue SP-A in the Nano-SiO$_2$ group was probably transferred into the bloodstream.
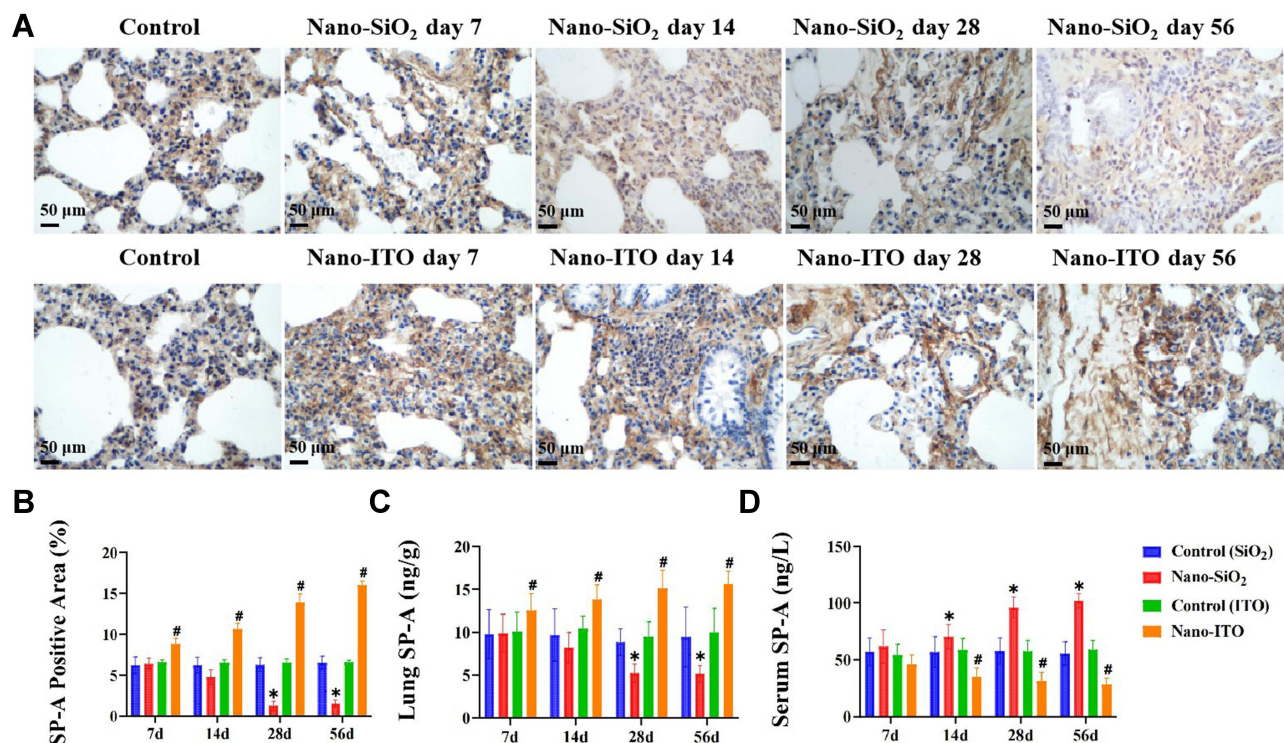
Figure 7 Expression and level of SP-A in lung tissue and serum. (**A**) Immunohistochemical staining for SP-A shows positive staining for proteinaceous materials, type II alveolar epithelial cells, alveolar macrophages, and alveolar mucus. Magnification ×200. Scale bar indicates 50 μm. (**B**) Graph of the mean area % of immunoreaction to SP-A. (**C**) SP-A levels in lung tissue at four time points. (**D**) SP-A levels in serum at four time points. Results are expressed as mean ± SD and analyzed using One Way ANOVA followed by Bonferroni's post-hoc test at $P < 0.05$ (n = 4–8). *$P < 0.05$, Nano-SiO$_2$ vs control, #$P < 0.05$, Nano-ITO vs control.
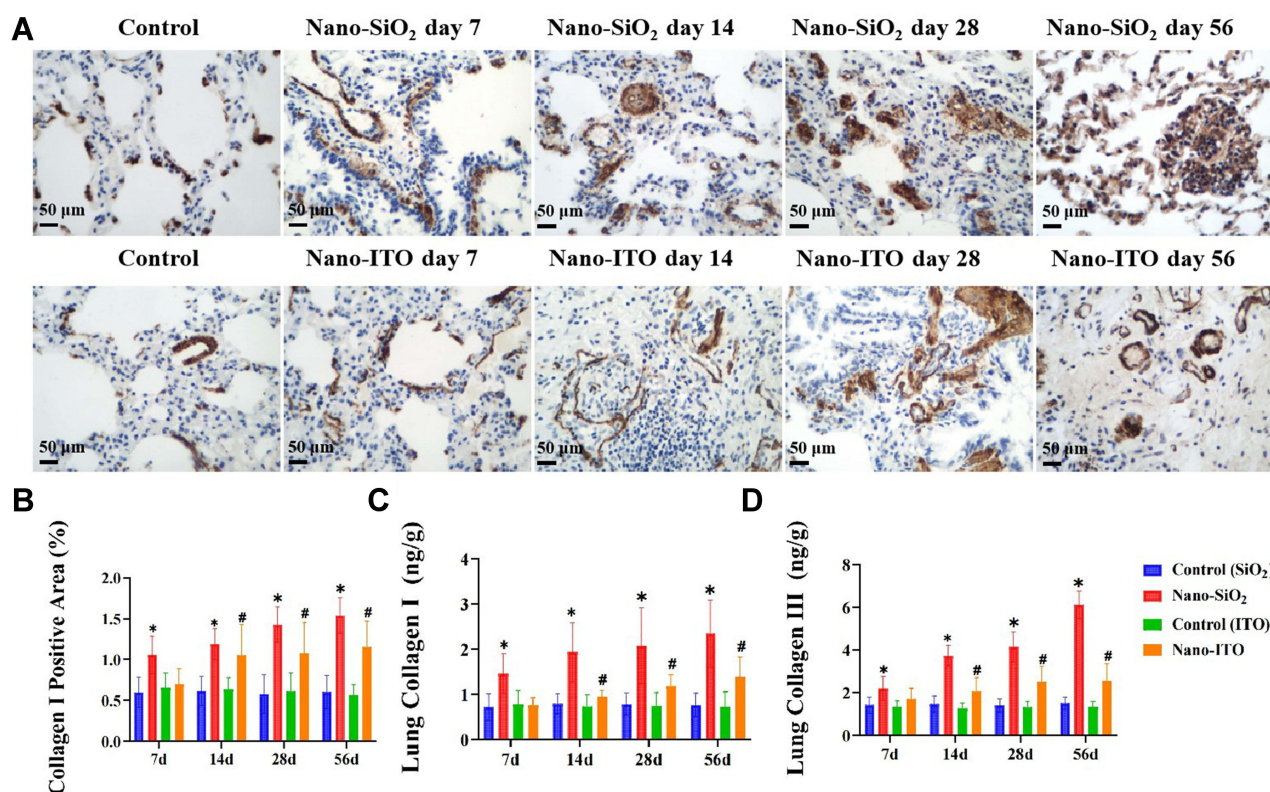
Figure 8 Expression and levels of collagen type I and collagen type III in lung tissues of Nano-SiO$_2$ and Nano-ITO rats. (**A**) Immunohistochemical staining for collagen type I on the lung tissue. Magnification ×200. Scale bar indicates 50 μm. (**B**) Graph of the mean area % of immunoreaction to collagen type I. (**C**) Collagen type I levels in lung tissue at four time points. (**D**) Collagen type III levels in lung tissue at four time points. Results are expressed as mean ± SD and analyzed using One Way ANOVA followed by Bonferroni's post-hoc test at $P < 0.05$ (n = 4–8). *$P < 0.05$, Nano-SiO$_2$ vs control, #$P < 0.05$, Nano-ITO vs control.

Deposition of Collagen Type I and III in the Lung

Immunohistochemistry and ELISA were used to detect the expression of collagen type I and collagen type III in lung tissues of Nano-SiO$_2$ and Nano-ITO. The immunostained lung section examination demonstrated that there were only a small number of collagen type I positive cells in the control group, mainly around bronchus and blood vessels. Compared with the control group, the expression of collagen type I in the lung tissue of the Nano-SiO$_2$ group increased in a time-dependent manner (Figure 8A and B). We further verified this result by analyzing the relative contents of collagen type I and collagen type III in lung tissues by ELISA. The results showed that, in response to Nano-SiO2 that had been instilled seven days prior, the relative contents of collagen type I and collagen type III in lung tissues increased dramatically (Figure 8C and D). One of the most important functions of myofibroblasts is to secrete extracellular matrix. Masson's trichrome staining showed that compared with the control group, the lungs in the Nano-SiO2 group had higher collagen accumulation (Figure 8A). The above data showed that Nano-SiO$_2$ accelerates pulmonary fibrosis in male Sprague-Dawley rats. Concerning the collagen deposition levels, the relative contents of collagen type I and collagen type III in the Nano-ITO group also increased significantly, the results are consistent with results from the Nano-SiO$_2$ groups.

Discussion

Silicosis is an occupational disease caused by massive or acute inhalation of silica, which is characterized by progressive pulmonary fibrosis. The pathological types of silicosis include simple (nodular) silicosis, progressive massive fibrosis, and diffuse interstitial fibrosis.[15] Indium lung is a new type of lung injury, first reported in 2003, leads to high rates of morbidity and mortality.[16] Current research shows that indium lung disease is a newly discovered, potentially fatal occupational disease. Its main feature is PAP, which may progress to fibrosis with or without emphysema. These findings

were consistent with our results in Nano-SiO$_2$ and Nano-ITO exposure models, which proved an effective method to simulate silicosis and PAP by intratracheal instillation.

For the intratracheal instillation in the present study, we used 50 mg/kg of Nano-SiO$_2$ and 6 mg/kg of Nano-ITO. In our previous intratracheal instillation studies, 6 mg/kg of Nano-ITO, was the maximum dose for inducing persistent lung inflammation, eventually lead to pulmonary fibrosis and alveolar proteinosis in rat lungs,[13] while 50 mg/kg of Nano-SiO$_2$, was the appropriate dose to induce fibrosis. The results of those studies reveal that pulmonary toxicity following intratracheal instillation can be evaluated by using those dose rates, avoiding excessive dose which produced not only toxicity of Nano-SiO$_2$ or Nano-ITO itself, but also additional negative effects. As this study describes, from the basis of previous work, 50 or 6 milligrams per rat in intratracheal instillation was considered to not reach excessive dose.

To explore and compare pulmonary injury effect of Nano-SiO$_2$ and Nano-ITO, in our study, rats were exposed to Nano-SiO$_2$ or Nano-ITO. At four different time points, rat lung tissues were collected for histopathological examination by H&E staining, Masson's trichrome staining, sirius red staining, PAS staining, TEM, and immunohistostaining which can be used to explain the difference that exists between the Nano-SiO$_2$-induced model and Nano-ITO-induced model in rats. It was found in the present study that intratracheal instillation of Nano-SiO2 mainly caused inflammation, granuloma, AMs mobilization, and pulmonary fibrosis (Figure 3A). In contrast, the inflammatory reaction or related histopathological damage induced by Nano-ITO showed that agglutinated particles surrounded by epithelial cells and a large amount of AMs continued to appear in the bronchiolar and alveolar ducts throughout the whole observation period of 56 days, which was characterized by the expansion of alveolar airspaces by PAS positive proteinaceous secretions, and was considered to be a form of secondary PAP (Figure 4B). The present result of the Nano-ITO-induced PAP is similar to those previously reported, that is, repeated instillation of Nano-ITO of the same sizes in rat trachea can induce significant PAP and foamy and degenerative AMs.[13,17]

In comparing the lung response of Nano-SiO$_2$ and Nano-ITO, based on histopathological examination, both similarities and differences in pathological changes were observed. For example, the Nano-ITO caused increased inflammatory changes in lung tissue in the same manner as observed with Nano-SiO$_2$ in comparison to the control (Figure 3). Our results showed that exposure to Nano-ITO induced significant acute and chronic lung inflammation that was characterized by the infiltration of abundant foamy macrophages and neutrophils into the pulmonary parenchyma. In Nano-SiO$_2$ affected rat lung tissue, granulomatous inflammation was the most remarkable lung lesion followed by progressive massive fibrotic nodules, in conjunction with bronchioloalveolar hyperplasia, interstitial fibrosis, alveolar inflammatory cell infiltration, fibrosing alveolitis, and fibropleurisy. Although persistent chronic inflammation and fibrosis were also observed in the lungs exposed to Nano-ITO, their severity was much lower than that exposed to Nano-SiO$_2$. For Nano-SiO$_2$, the changes appeared earlier and persisted longer. In the Nano-ITO study, PAP was observed with signs of inflammation (pneumonia, alveolar and bronchiolar hyperplasia) and fibrosis. PAP increased up to the end of the 56th day. In contrast, Nano-SiO$_2$ at the same exposure time did not cause signs of alveolar proteinosis material, but there were still substantial amounts silicosis nodules suggesting that the pathophysiological mechanisms of Nano-SiO$_2$ and Nano-ITO are different. The Nano-SiO$_2$ and Nano-ITO-induced pulmonary fibrosis was further confirmed by Masson's trichrome staining and sirius red staining (Figure 4). To sum up, our research shows that both Nano-SiO$_2$ and Nano-ITO can cause pulmonary injury and inflammation, but the degree of lung toxicity is different.

Based on the pathophysiological features of Nano-SiO$_2$ and Nano-ITO affected rats, we defined the progression of silicosis and PAP in rats as inflammatory stage, fibrotic stage and proteinosis stage. The inflammatory stage is characterized by a significant increase in lung inflammation. At this stage, some inflammation-related parameters, such as the expression of inflammatory cytokines (IL-6 and TNF-α) in BALF and lung tissue, were significantly up-regulated. The fibrotic stage showed severe lung fibrosis. Specifically, typical silicotic nodules revealed by Masson's trichrome staining and sirius red staining in the lung tissue sections of rats in the Nano-SiO$_2$ group were similar to silicosis lesions in human. In these nodules, the cavity center of deposited Nano-SiO$_2$ was surrounded by collagen fibers and dust laden macrophages. In addition, the expression of fibrotic markers including collagen type I and collagen type III reached the highest level in this stage. In the stage of proteinosis, the denaturation and injury of particle rich AMs lead to the accumulation of pulmonary surfactant. Specifically, the typical cholesterol crystals shown by PAS staining are similar to

those of human indium lung disease. In addition, increased expression of SP-A was confirmed by immunohistochemistry and ELISA in the lungs of the Nano-ITO affected rats.

Silicosis is a progressive process, depending on the amount of collagen synthesis controlled by related genes. The protein contents of collagen type I and collagen type III increased significantly in lung fibrosis; they are often known as indicators of lung fibrosis.[18] This feature also appeared in the Nano-SiO$_2$ exposure model rats in this study. The present study also proved that inflammation was involved in the occurrence and development of silicosis. In the early stage of rat silicosis model induced by Nano-SiO$_2$, the pulmonary inflammatory reaction was severe, levels of TNF-α and IL-6 increased significantly, while the degree of pulmonary fibrosis was mild. In a later stage, the inflammatory reaction was reduced, levels of TNF-α and IL-6 decreased, whereas the degree of pulmonary fibrosis was aggravated. In addition, Masson's trichrome staining revealed that there was severe pulmonary fibrosis in Nano-SiO$_2$-treated lung tissues, which was specifically manifested as typical silicosis nodules, and collagen fibers were arranged in concentric circles (Figure 4A). The expression of collagen type I and collagen type III also increased significantly. In conclusion, our results indicated that these markers (TNF-α, IL-6, collagen type I and collagen type III) can be used to reflect the overall progress of silicosis in rats. In addition, these findings also distinguished some pathophysiological characteristics of pulmonary inflammation and fibrosis in Nano-SiO$_2$ affected rats. The typical silicotic nodule with central cavitation was observed at day 14. Severe pulmonary fibrosis was observed at day 28; indicated by the up-regulated fibrosis markers (collagen type I and collagen type III). Taken together, these results suggested that short-time (seven days) exposure of Nano-SiO$_2$ could induce lung inflammation. In contrast, prolonged exposure (14–56 days) could lead to severe lung fibrosis in rats. With the combined use of histopathological analysis, immunohistochemistry, collagen type I and III concentration determination, Masson's trichrome staining, and sirius red staining we found that Nano-SiO2 accelerated the formation of pulmonary fibrosis and granulomatous inflammation in Sprague-Dawley rats.

The relationship between proteinosis and lung inflammation and fibrosis is still unclear in the occurrence and development of indium lung disease. Current research results showed that Nano-ITO exposure mainly induced significant lung inflammation in the early stage (seven days). However, no remarkable pulmonary proteinosis was apparent in the early stage. Soon afterwards, with the aggravation of lung inflammation, pulmonary fibrosis appeared significantly on day 14. More importantly, accumulations of intra-alveolar lightly eosinophilic finely granular materials were also appeared on day 14 and continued to deteriorate in the fibrotic stage. Longer term effects of instilled Nano-ITO in rats (56 days) were also manifested in pulmonary parenchymal inflammation, vacuolar alveolar macrophages, alveolar fibrin accumulation, and peribronchial fibrosis. These observations reveal that in the Nano-ITO rat model, the aggravation of pulmonary fibrosis caused by persistent lung inflammation may be the main reason for inducing PAP. Moreover, increased expression of SP-A was confirmed by immunohistochemistry and ELISA in the lungs of Nano-ITO affected rats, which suggested that increased SP-A expression of type II epithelial cells are related to the the development process of PAP during pulmonary fibrosis. It is currently accepted that surfactant is the main component of PAP, which is produced by the overproduction of alveolar type II epithelial cells and/or the interference of type II cells and alveolar macrophages in the removal process. In this study, excessive precipitation of protein substances in the alveolar space was determined as PAP, since these substances were PAS-positive and the TEM images of the lungs from the Nano-ITO-instilled group also showed multilayer, lattice and myelin-like structures. It has been reported that surfactant catabolism and AMs clearance may be involved in the pathogenesis of PAP.[19] In the present study, the degeneration and injury of Nano-ITO-laden AMs resulting in accumulation of pulmonary surfactant appeared in the lungs from the Nano-ITO-instilled group. We believe that there is a causal relationship between the PAP induced by Nano-ITO and the impairment of the lung surfactant metabolism caused by defective AMs. Taking into consideration our results of a significant increase of TNF-α and IL-6 in BALF from rats with PAP together with the significant expression of SP-A in lungs, it can be inferred that the marked elevation in TNF-α and IL-6 levels in the BALF from the Nano-ITO-instilled group is closely related to AMs deficiency, which is due to the enhanced phagocytosis of Nano-ITO in the alveolar space. Combined with histopathology, immunohistochemistry, SP-A concentration measurement, and PAS staining we found that Nano-ITO accelerated the formation of PAP in the lungs of Sprague Dawley rats, accompanied by granulomatous inflammation and fibrosis.

In the present study, some common histopathological characteristics of lung were found in Nano-SiO$_2$ and Nano-ITO exposed rats. In the fibrosis stage, severe pulmonary fibrosis appeared, including thickening of alveolar wall and forming of cellulosic nodules in the alveolar matrix. In addition, several markers of pulmonary inflammation and fibrosis

significantly increased in both Nano-SiO2 and Nano-ITO exposed rats and reflected in increased LDH activity and total protein concentration in BALF, which was also confirmed by histopathological examination. In conclusion, the similar pathophysiological characteristics that we observed in Nano-SiO$_2$ and Nano-ITO exposed rats revealed that the early pathophysiological processes found in the silicosis models may also exist in PAP models, which needs further confirmation. Exposure at 50 mg/kg for seven days in Nano-SiO$_2$ exposed rats and 6 mg/kg for seven days in Nano-ITO exposed rats might be appropriate conditions to induce silicosis and PAP into the inflammatory stage. To induce the progressive stage, 50 mg/kg of Nano-SiO$_2$ for 14 days and 6 mg/kg of Nano-ITO for 14 days in rats may be the appropriate choice. To induce the fibrotic stage, exposure to Nano-SiO$_2$ at 50 mg/kg for 28 days or Nano-ITO at 6 mg/kg for 14 days in rats is sufficient. For the proteinosis stage, exposure to Nano-ITO at 6 mg/kg for 28 days is sufficient.

Conclusions

In conclusion, we successfully established two rat models of Nano-SiO$_2$ (silicosis) and Nano-ITO (indium lung) and analyzed the pathological characteristics. Our study revealed pathological characteristics in different stages of both silicosis rats and indium lung rats; this validates the reasoning for the study. Silicosis rat model and PAP rat model were different in terms of pathological features. Moreover, the Nano-SiO$_2$-induced model has greater value for research on granulomas and fibrosis, while the Nano-ITO-induced model has greater repeatability in the area of PAP. This is the first study to comparatively analyze the differences, which may provide information for choosing between the silicosis model or the indium lung disease model. We hope that the models of this study will be used to explore the specific pathogenesis of silicosis and indium lung, and provide more theoretical support for the later treatment of occupational patients.

Disclosure

All authors declare that there are no conflicts of interest regarding the publication of this article.

References

1. De Matteis S, Heederik D, Burdorf A, et al. Current and new challenges in occupational lung diseases. *Eur Respir Rev*. 2017;26(146):170080. doi:10.1183/16000617.0080-2017
2. Kumar A, Cummings KJ. Pulmonary alveolar proteinosis secondary to occupational exposure. *Curr Pulmonol Rep*. 2021;10:30–39. doi:10.1007/s13665-021-00267-1
3. Lison D, Laloy J, Corazzari I, et al. Sintered indium-tin-oxide (ITO) particles: a new pneumotoxic entity. *Toxicol Sci*. 2009;108(2):472–481. doi:10.1093/toxsci/kfp014
4. Badding MA, Stefaniak AB, Fix NR, et al. Cytotoxicity and characterization of particles collected from an indium-tin oxide production facility. *J Toxicol Environ Health A*. 2014;77(20):1193–1209. doi:10.1080/15287394.2014.920757
5. Huaux F, De Gussem V, Lebrun A, et al. New interplay between interstitial and alveolar macrophages explains pulmonary alveolar proteinosis (PAP) induced by indium tin oxide particles. *Arch Toxicol*. 2018;92(4):1349–1361. doi:10.1007/s00204-018-2168-1
6. Hamilton RF, Thakur SA, Holian A. Silica binding and toxicity in alveolar macrophages. *Free Radic Biol Med*. 2008;44(7):1246–1258. doi:10.1016/j.freeradbiomed.2007.12.027
7. Okamoto M, Tominaga M, Shimizu S, et al. Dental technicians' pneumoconiosis. *Intern Med*. 2017;56(24):3323–3326. doi:10.2169/internalmedicine.8860-17
8. Amata A, Chonan T, Omae K, et al. High levels of indium exposure relate to progressive emphysematous changes: a 9-year longitudinal surveillance of indium workers. *Thorax*. 2015;70(11):1040–1046. doi:10.1136/thoraxjnl-2014-206380
9. Guha N, Loomis D, Guyton KZ, et al. Carcinogenicity of welding, molybdenum trioxide, and indium tin oxide. *Lancet Oncol*. 2017;18(5):581–582. doi:10.1016/S1470-2045(17)30255-3
10. Cummings KJ, Donat WE, Ettensohn DB, et al. Pulmonary alveolar proteinosis in workers at an indium processing facility. *Am J Respir Crit Care Med*. 2010;181(5):458–464. doi:10.1164/rccm.200907-1022CR

11. Subhadarshini S, Singh R, Mandal A, et al. Silver nanodot decorated dendritic copper foam as a hydrophobic and mechano-chemo bactericidal surface. *Langmuir.* 2021;37(31):9356–9370. doi:10.1021/acs.langmuir.1c00698

12. Subhadarshini S, Pavitra E, Raju GSR, et al. One-pot facile synthesis and electrochemical evaluation of selenium enriched cobalt selenide nanotube for supercapacitor application. *Ceram Int.* 2021;47(11):15293–15306. doi:10.1016/j.ceramint.2021.02.093

13. Liu N, Guan Y, Zhou C, et al. Pulmonary and systemic toxicity in a rat model of pulmonary alveolar proteinosis induced by indium-tin oxide nanoparticles. *Int J Nanomedicine.* 2022;17:713–731. doi:10.2147/IJN.S338955

14. Li S-X, Li C, Pang X-R, et al. Metformin attenuates silica-induced pulmonary fibrosis by activating autophagy via the AMPK-mTOR signaling pathway. *Front Pharmacol.* 2021;12:719589. doi:10.3389/fphar.2021.719589

15. Anlar HG, Bacanli M, Iritaş S, et al. Effects of occupational silica exposure on oxidative stress and immune system parameters in ceramic workers in Turkey. *J Toxicol Environ Health A.* 2017;80(13–15):688–696. doi:10.1080/15287394.2017.1286923

16. Toshiaki H, Takahiro U, Kiyohisa S, et al. Interstitial pneumonia developed in a worker dealing with particles containing indium-tin oxide. *Joccup Health.* 2003;45:137–139. doi:10.1539/joh.45.137

17. Liu N, Li G, Gai Y, et al. N-acetylcysteine alleviates pulmonary alveolar proteinosis induced by indium-tin oxide nanoparticles in male rats: involvement of the NF-κB signaling pathway. *Ecotoxicol Environ Saf.* 2022;241:113812. doi:10.1016/j.ecoenv.2022.113812

18. Zhang B-N, Zhang X, Xu H, et al. Dynamic variation of RAS on silicotic fibrosis pathogenesis in rats. *Curr Med Sci.* 2019;39(4):551–559. doi:10.1007/s11596-019-2073-8

19. Carey B, Trapnell BC. The molecular basis of pulmonary alveolar proteinosis. *Clin Immunol.* 2010;135(2):223–235. doi:10.1016/j.clim.2010.02.017